Cell Reports, Volume *30*

Supplemental Information

Structural Insights into Rational Design of Single-Domain Antibody-Based Antitoxins against Botulinum Neurotoxins

Kwok-ho Lam, Jacqueline M. Tremblay, Edwin Vazquez-Cintron, Kay Perry, Celinia Ondeck, Robert P. Webb, Patrick M. McNutt, Charles B. Shoemaker, and Rongsheng Jin

A

```
                                  CDR1                  CDR2                                                  CDR3
JEQ-H11    SGGGLVQAGGSLRLSCAGSGRS--FSAAVMGWFRQAPGKEREFVAALRQIIGSTHYADSVKGRFTISRDNAKNMLYLDMNSLKPTDTAAYYCTA------GPPTMLDVSTDREYDTWGQGTQVTVSS
JFM-A11    TGGGLVQPGGALRLSCAASVFG--MDYYYIGWVRQAPGKEREGVSCISN-IGRTHYADSVKGRFTISRDNAKNTVYLQMNSLKPEDTAVYYCAAA------PLVGNYCPASYEYESWGQGTQVTVSS
JFN-B5     SGGGLVQPGGSLRLSCAASGQS--LDNYIIGWFRQAPGKEREGVSCIDRTGTVTHYADSVKGRFTISTDNVKNTVYLEMNDLKPEDTATYFCAA---ERRWGVVSVCVISDYYFDSWGQGTQVTVSS
JFM-B9     TGGGLVQAGGSLRLSCTASGRT--SSFYALAWFRQGPGKEREFVAAIGWIDGSTRYTDSAKGRFTISRDAAKNTMYLQMNSLKPEDTAVYSCTA------RTQYGGSSADPKNYGYWGQGTQVTVSA
JLI-G10    SGGGLVQPGGSLRLSCAASILTYDLDYYYIGWVRQAPGKEREGVSCISSTDGATYYADSVKGRFTISRNNAKNTVYLQMNNLKPEDTAIYYCAA------APLAGRYCPASHEYGYWGQGTQVTVSS
JLI-H11    SGGGLVQPGESLRLSCGASGMS--LDYYAIAWYRQAPGKEREGVSCISVSGSSAQYLDSVRGRFIISKDNTKSTAYLQMNSLKPEDTAVYYCAA------LADCAGYASLTFDFDSWGQGTQVAVSS
JLJ-F9     SGGGLVQAGGSLRLSCAPSRLT--LDFFAIAWFRQAPGKEREGVSCISSHDGSTYYTDSVKGRFTISKDNAKNTVYLQMNSLKPEDTAVYYCAL------DHNVGTCQLTQAEYDYWGQGTQVTVSS
JLJ-G3     SGGGLVQSGGSLRLSCAASGSI--DSLYHMGWYRQAPGKERELVARVQD-GGSTAYKDSVKGRFTISRDFSRSTMYLQMNSLKPEDTAIYYCAA-------------KSTISTPLSWGQGTQVTVSS
JLK-D7     SGGGLVQAGGSLRLSCAASGFT--LGHNQVAWFRQAPGKEREGVACISATGASTHYADPVKGRFTVSRDNTKNVVYLQVNSLKPEDTANYVCAS--RFSLMSIDASMCLSAPQYDRWGQGTQVRISS
JLK-G12    SGGGLVQAGGSLRLSCAASEFR--AEHFAVGWFRQAPGKEREGVSCVDASGDSTAYADSVKGRFTISRDNNKNVVYLQMDSLEPEDTGDYYCGA-----SYFTVCAKSMRKIEYRYWGQGTQVTVSS
JLO-C8     SGGGLVQPGGSLRLSCAASGRA--LNYYVIGWFRQAPGKEREGVSCIASSEAYTDYADSVQGRFTISRDKALNTVYLDMKRLKPDDTAVYYCAA-----RLRDPNWCGRNADEYDSWGQGTQVTVSS
JLO-G7     SGGGLVQAGGSLRLSCAASGFP--FGSYYMSWVRQAPGKGPEWVSDISNGGIITRYSDSVKGRFTISRDNAKNILYLQMNSLKPEDTALYFCAT------------GTGRDWSREYRGQGTQVTVSS
JLO-G11    SGGGLVQPGGSLRLSCEASGFH--LEHFAVGWFRQAPGKEREGVSCISASGDSTTYADSVKGRSTISKDNAKNAVYLQMDSLRPEDTGDYYCAA-----SHFSVCGKNIRKIEYRYWGQGTPVTVSS
JLU-D10    SGGGLVQPGGSLRLSCAASGFT--LDSYAIGWFRQAPGKEREGVACISASGSGTDYVDSVKGRFTVSRDQAKSMVFLQMNNMKPEDAAVYYCAA--DYRPRPLPIQAPCTMTGGNYWGQGTQVTVSS
JLU-H9     SGGGLVQPGGSLRLSCAAPGFT--LDYYAIGWFRQAPGKEREGVSCIRSRGDRTNYADSVKGRFTVSRDNAKNTAYLQMNNLKPEDTGVYFCAAAPRTTVQDLCVTPLLGGADWVSWGQGTQVTVSS
JLU-H10    SGGGLVQPGGSLRLSCAASGFP--LGDYTVGWFRQAPGKEREGVSCISKGSRGLRYGDSVKGRFTVARDNAKSTVTLQMDSLKPEDTAVYSCAA-----GPAMFNQCHMVDNYFTYWGQGTQVTVSS
JNE-B10    SGGGLVQPGGSLRLSCAASGFP--FHAYYMSWVRQAPGKGLEWVSHIGNGGIITRYADSVKGRFTISRDNAKNTLYLQMTNLKPEDTALYYCTL-------------GTRDDLGPERGQGTQVTVSS
```

B

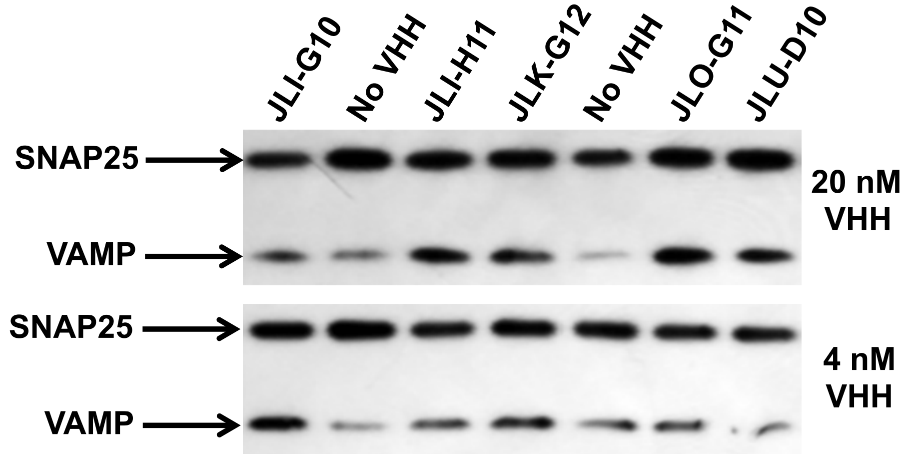

Figure S1. Amino acid sequences and characterization of anti-BoNT/B1 VHHs. Related to Figure 2.
(A) Amino acid sequences of anti-BoNT/B1 VHHs. The amino acid sequences of VHH JEQ-H11, JFM-A11, JFN-B5, and JFM-B9 were reported in our previous study (Mukherjee et al., 2012) and were listed here for comparison.
(B) VHH neutralization of BoNT/B1 in rat primary cerebellar neuron cultures. Purified VHHs were added to cell culture media of cerebellar primary neurons at the indicated concentrations and then 1 nM of BoNT/B1 or medium control was added. After overnight incubation, the extent of VAMP cleavage was assessed by Western blot.

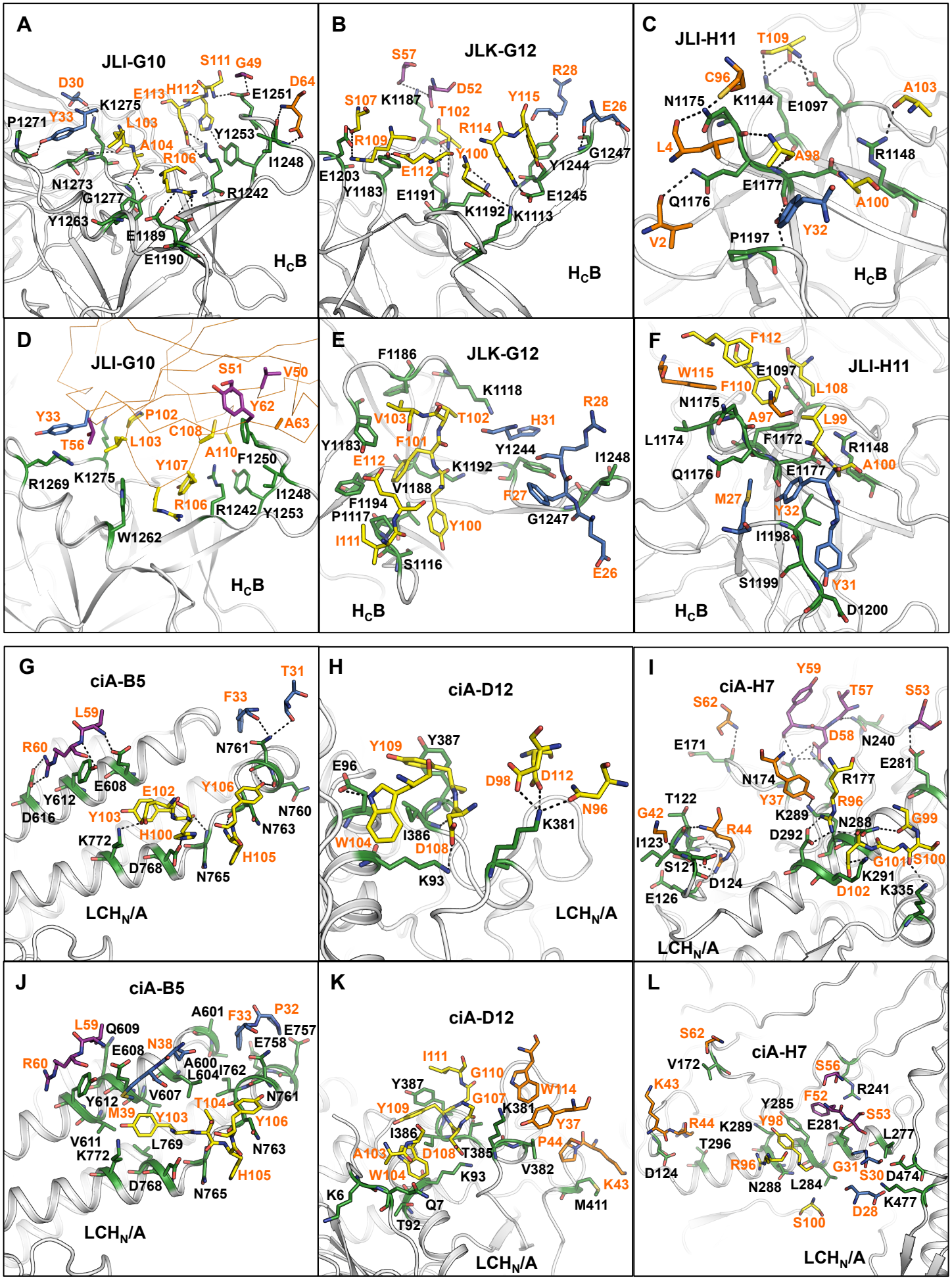
A
JLI-G10
D30
S111
G49
E113
H112
D64
K1275
E1251
P1271
Y33
L103
Y1253
A104
R106
I1248
N1273
R1242
G1277
Y1263
E1189
E1190
H_CB
B
JLK-G12
S57
R28
D52
S107
K1187
Y115
E26
T102
R114
R109
Y100
G1247
E112
Y1244
E1203
Y1183
E1191
E1245
K1192
K1113
H_CB
C
JLI-H11
T109
C96
A103
N1175
K1144
E1097
L4
A98
R1148
E1177
Q1176
A100
V2
Y32
P1197
H_CB
D
JLI-G10
S51
V50
Y62
Y33
P102
A63
C108
T56
L103
A110
F1250
Y107
R1269
K1275
I1248
R106
R1242
Y1253
W1262
H_CB
E
JLK-G12
F1186
K1118
R28
V103
T102
H31
Y1183
F101
Y1244
I1248
E112
K1192
V1188
F27
F1194
P1117
G1247
Y100
I111
S1116
E26
H_CB
F
JLI-H11
F112
W115
E1097
F110
L108
N1175
A97
L99
L1174
F1172
R1148
Q1176
E1177
A100
M27
Y32
I1198
S1199
Y31
D1200
H_CB
G
ciA-B5
T31
F33
L59
R60
N761
E608
Y612
E102
Y106
D616
Y103
N760
H100
N763
K772
H105
D768
N765
LCH_N/A
H
ciA-D12
Y109
Y387
E96
D98
D112
N96
K381
W104
I386
D108
K93
LCH_N/A
I
ciA-H7
Y59
S62
T57
S53
D58
N240
E171
E281
N174
R177
T122
Y37
R96
G42
K289
N288
G99
R44
D292
I123
S121
G101
S100
D124
K291
D102
K335
E126
LCH_N/A
J
ciA-B5
A601
F33
P32
L59
Q609
E757
N38
E608
E758
R60
A600
L604
I762
V607
Y612
T104
N761
M39
Y103
Y106
V611
L769
N763
K772
H105
D768
N765
LCH_N/A
K
ciA-D12
I111
G110
Y387
W114
G107
Y109
K381
Y37
I386
P44
A103
D108
T385
V382
W104
K93
K43
K6
Q7
M411
T92
LCH_N/A
L
ciA-H7
S62
V172
S56
K43
R241
F52
Y285
S53
R44
K289
Y98
E281
L277
T296
D124
R96
G31
S30
D474
N288
L284
D28
K477
S100
LCH_N/A

Figure S2. Molecular interactions between H_CB or LCH_N/A and VHHs. Related to Figures 2–4. Residues mediating electrostatic interactions (**A–C, G–I**) or hydrophobic interactions and van de Waal forces (**D–F, J–L**) between the toxin fragments and VHHs are shown as sticks. The VHH-binding epitopes on H_CB or LCH_N/A are colored green. The interacting residues in the CDR1, 2, 3 loops and the framework region of the VHHs are colored blue, purple, yellow, and orange respectively.

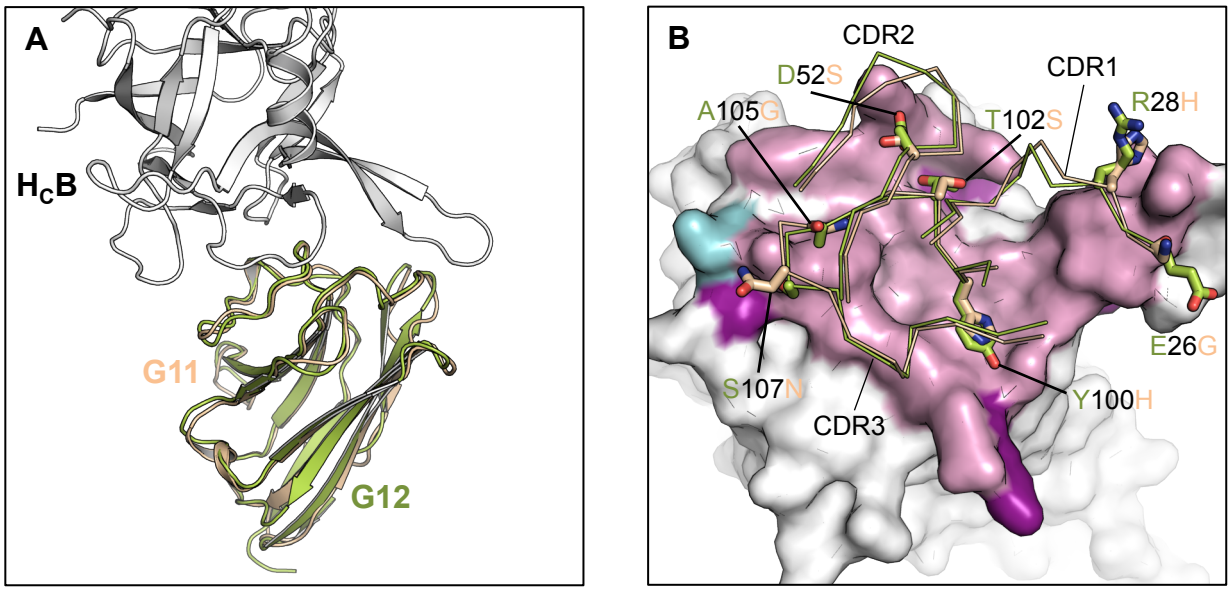

Figure S3. Structure of the H_CB–JLO-G11 complex. Related to Figure 2.
(A) Structural superposition between the H_CB–JLO-G11 and the H_CB–JLK-G12 complexes indicates that the binding mode of JLO-G11 is nearly identical to JLK-G12.
(B) JLO-G11 and JLK-G12 bind to nearly identical epitopes on H_CB. The JLO-G11- and JLK-G12-binding surfaces on H_CB are colored cyan and magenta, respectively, while the overlapping region is colored pink. The CDR loops of the VHHs are drawn as ribbons. The H_CB-interacting residues on JLO-G11 (wheat) and JLK-G12 (green) that are different between them are shown as sticks.

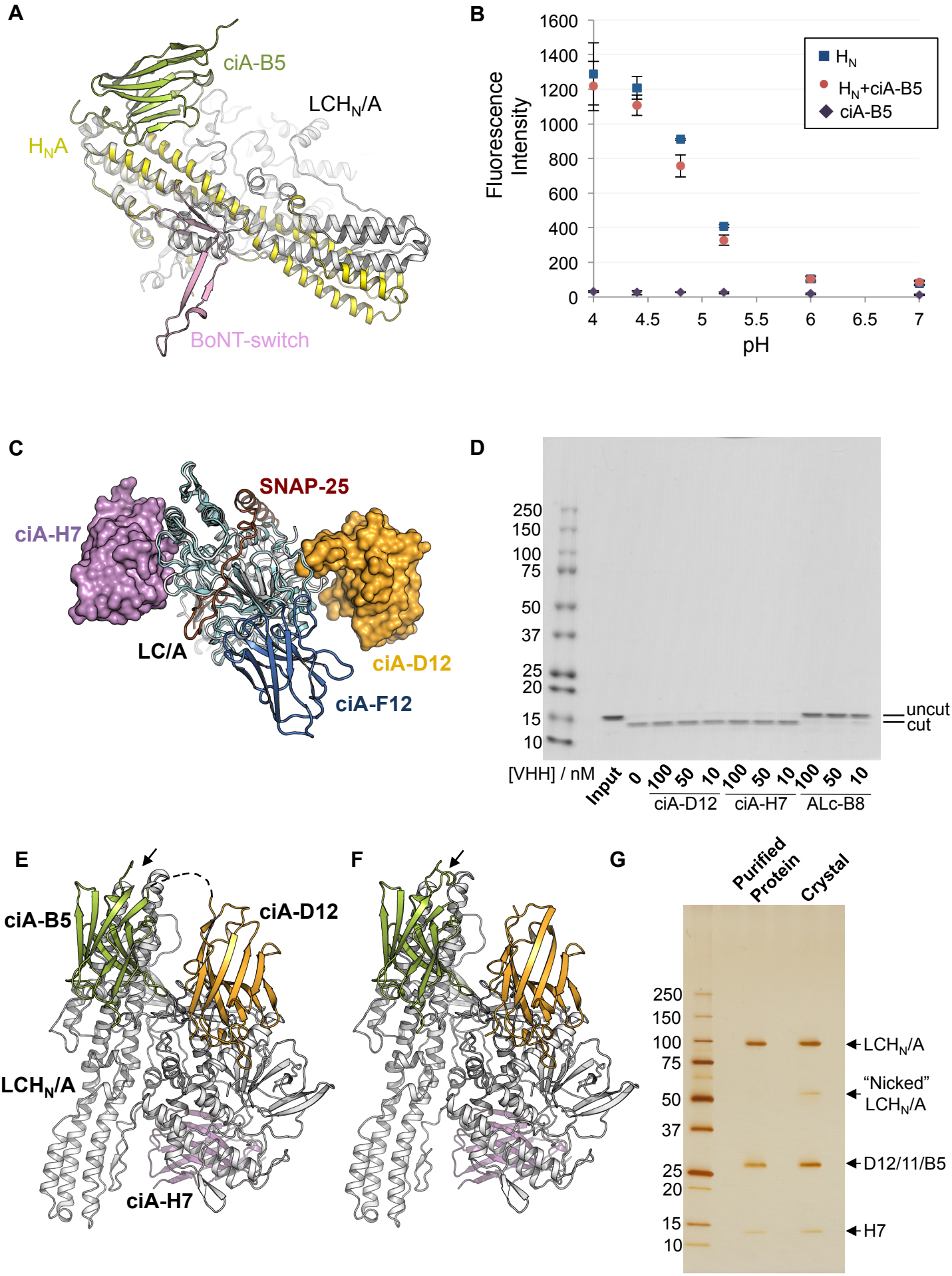
A
ciA-B5
LCHN/A
HNA
BoNT-switch
B
Fluorescence Intensity
1600
1400
1200
1000
800
600
400
200
0
4
4.5
5
5.5
6
6.5
7
pH
HN
HN+ciA-B5
ciA-B5
C
SNAP-25
ciA-H7
LC/A
ciA-D12
ciA-F12
D
250
150
100
75
50
37
25
20
15
10
uncut
cut
[VHH] / nM
Input
0
100
50
10
100
50
10
100
50
10
ciA-D12
ciA-H7
ALc-B8
E
ciA-B5
ciA-D12
LCHN/A
ciA-H7
F
G
Purified Protein
Crystal
250
150
100
75
50
37
25
20
15
10
LCHN/A
"Nicked" LCHN/A
D12/11/B5
H7

Figure S4. Characterization of anti-BoNT/A VHHs. Related to Figures 3–5.

(A and B) VHH ciA-B5 has no effect on the structural change of the BoNT-switch.

(A) Structural superposition between the LCH_N/A–B5 complex and H_NA in the acidic-pH conformation (PDB code: 6DKK) indicates that the ciA-B5-binding epitope does not overlap with the BoNT-switch.

(B) ANS binding assay. H_NA, H_NA–ciA-B5, or ciA-B5 alone was incubated with ANS at 25 °C for 15 min. The peak fluorescence intensity at 466 nm is shown. Error bar represents SD of three replicate experiments.

(C and D) VHHs ciA-D12 and ciA-H7 do not affect the enzymatic activity of LC/A.

(C) Superimposing the structures of the LC/A–D12–H7 and the LC/A–SNAP-25 complexes indicates that D12 or H7 binding does not affect the LC/A–SNAP-25 interaction. Cartoon model of a non-neutralizing VHH ciA-F12 is drawn for comparison.

(D) In vitro SNAP-25 endopeptidase assay. LC/A (1 nM) was pre-incubated for 15 min with ciA-D12, ciA-H7, or a protease inhibitor ALc-B8 (10–100 nM) (Tremblay et al., 2010), respectively. The LC/A–VHH mixtures were then added to 5 mM of SNAP-25 (80–206) for 30 min at 25 °C. The gel image is a representative of three independent experiments.

(E–G) Crystal structure of the LCH_N/A–D12/11/B5–H7 complex.

Structures of the LCH_N/A–D12/11/B5–H7 (E) and LCH_N/A–B5–D12–H7 (F) complexes are drawn in the same orientation. These two structures are almost identical (r.m.s.d. of 0.212 over 956 aligned Cα atoms). Residues A26–P29 of ciA-B5 (arrow) and the 11-amino-acid peptide linker connecting ciA-D12 and ciA-B5 (dotted line) are not visible in the electron density map of the LCH_N/A–D12/11/B5–H7 complex. As shown in panel (G), D12/11/B5 remained intact during crystallization. Therefore, its peptide linker was present in the crystal, likely adopting a flexible conformation.

(G) Crystals of the LCH_N/A–D12/11/B5–H7 complex were isolated, washed five times with the mother liquor, and then denatured in SDS loading dye and analyzed by SDS-PAGE.

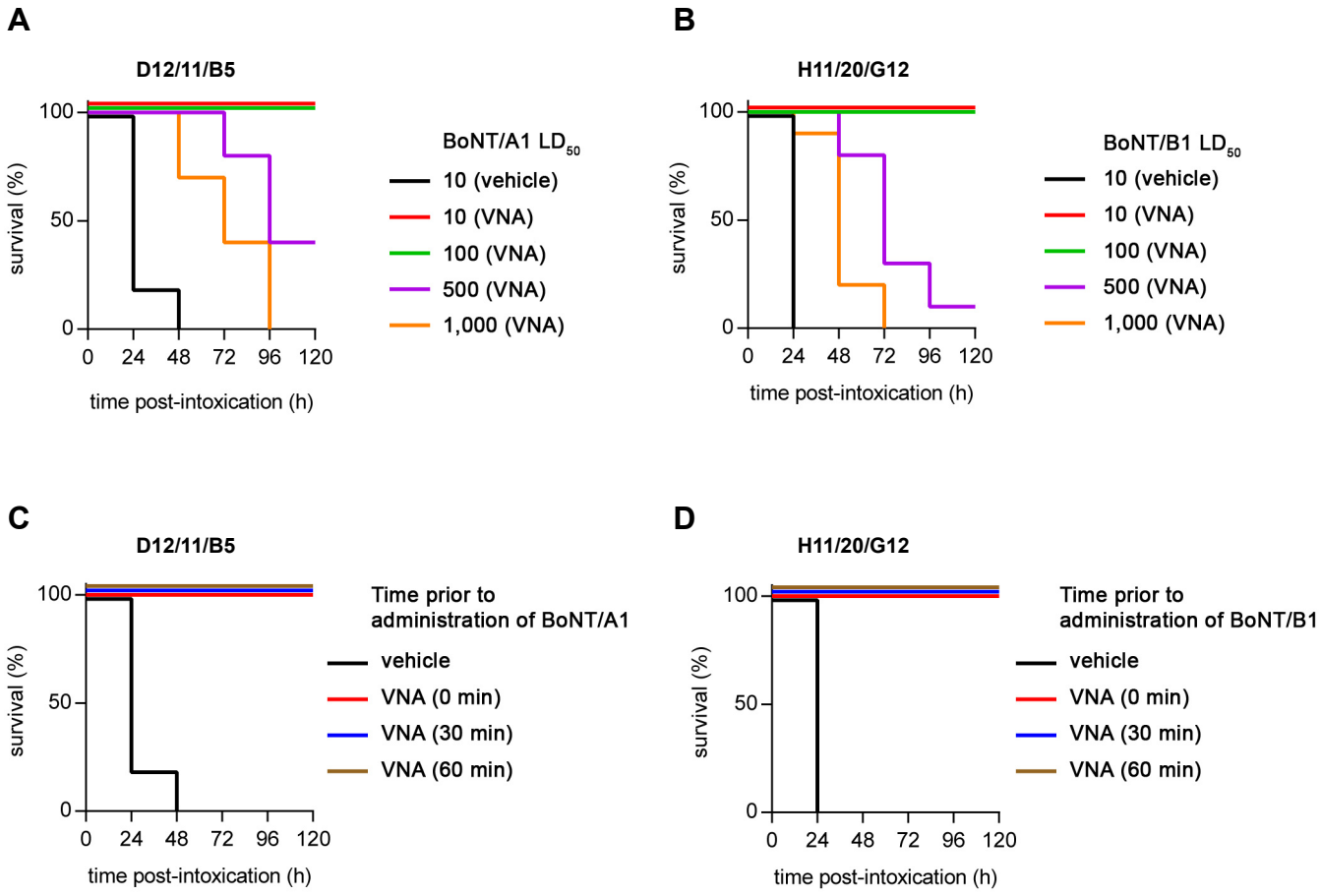

Figure S5. BoNT/A1 or BoNT/B1 intoxication in mice is prevented by separate administration of designer VNAs. Related to Figures 6–7.

(A and B) Symptoms of BoNT/A1 (A) or BoNT/B1 (B) intoxication and lethality were monitored following administration of bivalent VNA D12/11/B5 (A), H11/20/G12 (B), or toxin only. Time to death is plotted as % survival following IP injection of the indicated dose of toxin at 5 min after IV administration of VNAs in groups of five mice.

(C and D) VNA D12/11/B5 (C) and H11/20/G12 (D) were administered at indicated time points prior to injection of 10 LD_{50} of BoNT/A1 and BoNT/B1, respectively.

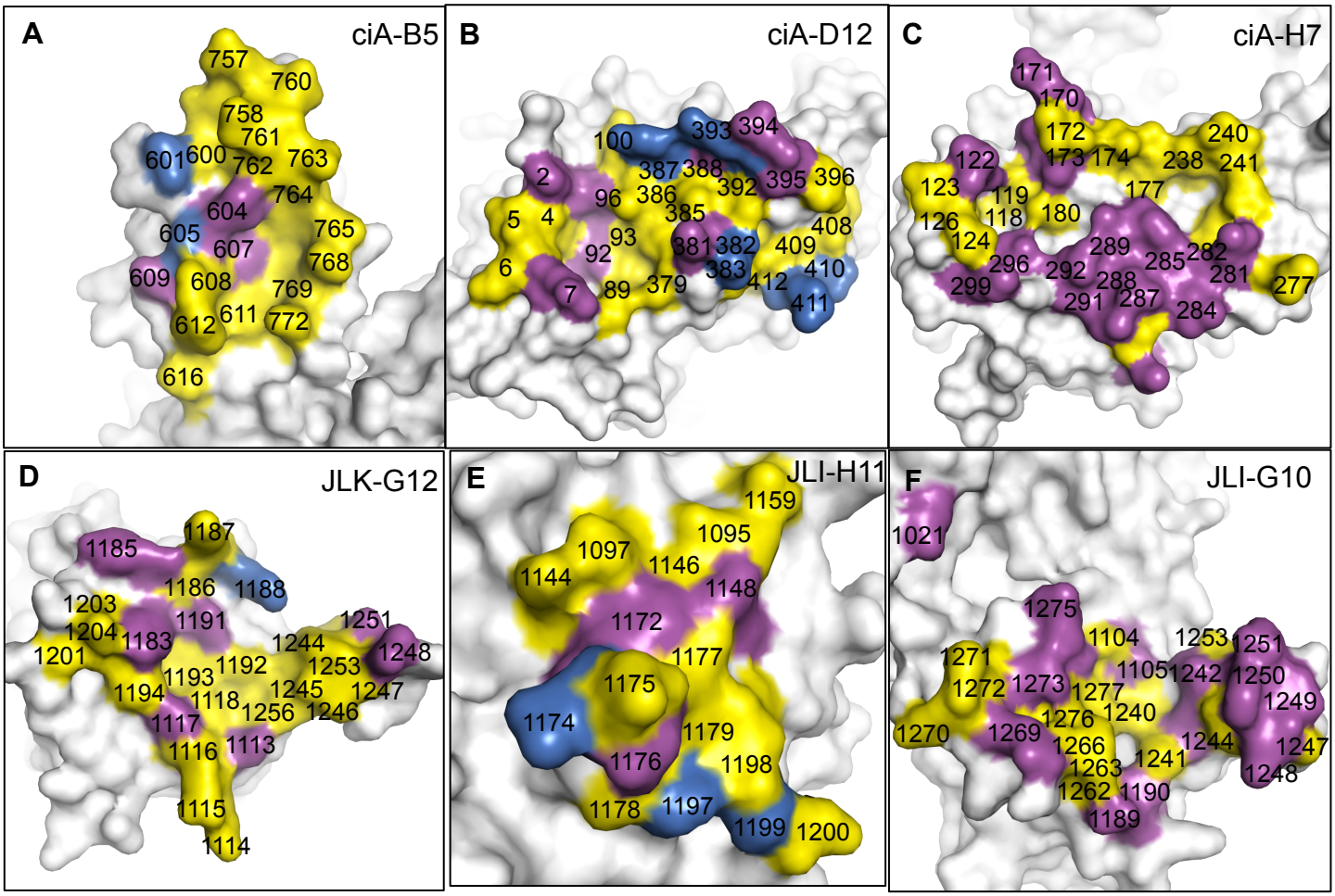

G ciA-B5

	% ID	% SIM
A1		
A2	80.95	90.48
A3	80.95	95.24
A4	76.19	95.24
A5	100.00	100.00
A6	100.00	100.00
A7	100.00	100.00
A8	100.00	100.00

	600	601	604	605	607	608	609	611	612	616	757	758	760	761	762	763	764	765	768	769	772
A1	A	A	L	G	V	E	Q	V	Y	D	E	E	N	N	I	N	F	N	D	L	K
A2	A	F	L	N	A	E	E	V	Y	D	E	E	N	N	I	N	F	N	D	L	K
A3	A	V	L	S	A	E	E	V	Y	D	E	E	N	N	I	N	F	N	D	L	K
A4	A	V	V	N	I	E	N	V	Y	D	E	E	N	N	I	N	F	N	D	L	K
A5	A	A	L	G	V	E	Q	V	Y	D	E	E	N	N	I	N	F	N	D	L	K
A6	A	A	L	G	V	E	Q	V	Y	D	E	E	N	N	I	N	F	N	D	L	K
A7	A	A	L	G	V	E	Q	V	Y	D	E	E	N	N	I	N	F	N	D	L	K
A8	A	A	L	G	V	E	Q	V	Y	D	E	E	N	N	I	N	F	N	D	L	K
consensus>70	A	.l	.	v	E	#	V	Y	D	E	E	N	N	I	N	F	N	D	L	K	

J JLK-G12

	% ID	% SIM
B1		
B2	80.77	80.77
B3	88.46	88.46
B4	69.23	73.08
B5	92.31	92.31
B6	88.46	88.46
B7	73.08	73.08
B8	73.08	80.77

	1113	1114	1115	1116	1117	1118	1183	1185	1186	1187	1188	1191	1192	1193	1194	1203	1204	1244	1245	1246	1247	1248	1251	1253	1256
B1	K	K	D	S	P	V	Y	Y	F	K	K	E	K	L	F	S	E	F	Y	E	S	G	I	E	Y
B2	K	K	D	S	S	V	Y	D	F	K	E	K	K	L	F	S	E	F	Y	E	S	G	I	K	Y
B3	K	K	D	S	S	V	Y	D	F	K	K	E	K	L	F	S	E	F	Y	E	S	G	I	K	Y
B4	V	K	D	S	S	V	Y	N	F	K	E	Q	K	L	F	S	E	F	Y	E	S	G	K	Y	V
B5	K	K	D	S	S	V	Y	Y	F	K	K	E	K	L	F	S	E	F	Y	E	S	G	I	K	Y
B6	K	K	D	S	P	V	L	N	F	K	K	E	K	L	F	S	E	F	Y	E	S	G	I	K	Y
B7	V	K	D	S	S	V	Y	N	F	K	G	E	K	L	F	S	E	F	Y	E	S	G	K	Y	I
B8	K	K	D	S	S	V	Y	D	F	K	G	Q	K	L	F	S	E	F	Y	E	S	G	Q	Y	F
consensus>70	k	K	D	S	s	V	y	d	F	K	.	e	K	L	F	S	E	F	Y	E	S	G	.	.	Y	y

H ciA-D12

	% ID	% SIM
A1		
A2	71.43	75.00
A3	57.14	64.29
A4	85.71	85.71
A5	92.86	92.86
A6	100.00	100.00
A7	96.43	96.43
A8	78.57	82.14

	2	4	5	6	7	89	92	93	96	100	379	381	382	383	385	386	387	388	392	393	394	395	396	408	409	410	411	412
A1	P	V	N	K	Q	K	T	K	E	S	V	K	V	N	T	I	Y	D	L	R	N	T	N	I	N	N	M	N
A2	P	V	N	K	Q	K	T	K	E	S	V	D	E	N	T	I	K	D	L	K	G	A	N	I	N	S	R	N
A3	P	V	N	K	P	K	I	K	D	S	V	D	E	N	T	I	N	E	L	E	G	A	N	I	N	S	R	N
A4	P	V	N	K	Q	K	I	K	F	S	V	D	V	N	T	I	H	D	L	R	N	T	N	I	N	N	K	N
A5	L	V	N	K	Q	K	T	K	E	S	V	E	V	N	T	I	Y	D	L	R	N	T	N	I	N	N	M	N
A6	P	V	N	K	Q	K	T	K	F	S	V	K	V	N	T	I	Y	D	L	R	N	T	N	I	N	N	M	N
A7	P	V	N	K	Q	K	T	K	E	S	V	E	V	N	T	I	Y	D	L	R	N	T	N	I	N	N	M	N
A8	P	V	N	K	Q	K	T	K	E	S	V	D	E	N	T	I	K	D	L	K	N	T	N	I	N	S	R	N
consensus>70	p	V	N	K	q	K	t	K	#	S	V	d	.	N	T	I	.	#	L	.	n	t	N	I	N	.	.	N

K JLI-H11

	% ID	% SIM
B1		
B2	76.47	76.47
B3	88.24	88.24
B4	70.59	76.47
B5	100.00	100.00
B6	100.00	100.00
B7	76.47	76.47
B8	82.35	88.24

	1095	1097	1144	1146	1148	1159	1172	1174	1175	1177	1178	1179	1197	1198	1199	1200
B1	N	E	K	I	R	D	F	L	N	Q	E	W	R	P	I	S	D
B2	N	E	K	I	R	D	F	S	N	R	E	W	R	N	I	Y	D
B3	N	E	K	I	R	D	F	L	N	Q	E	W	R	N	I	Y	D
B4	N	E	K	I	R	D	V	S	N	E	E	W	R	I	I	Y	D
B5	N	E	K	I	R	D	F	L	N	Q	E	W	R	P	I	S	D
B6	N	E	K	I	R	D	F	L	N	Q	E	W	R	P	I	S	D
B7	N	E	K	I	R	D	F	S	N	R	E	W	R	N	I	Y	D
B8	N	E	K	I	K	D	F	L	N	Q	E	W	R	N	I	H	D
consensus>70	N	E	K	I	r	D	f	.	N	q	E	W	R	.	I	.	D

I ciA-H7

	% ID	% SIM
A1		
A2	96.67	100.00
A3	63.33	70.00
A4	83.33	90.00
A5	96.67	100.00
A6	100.00	100.00
A7	90.00	96.67
A8	96.67	100.00

	118	119	121	122	123	124	126	170	171	172	173	174	177	180	238	240	241	277	281	282	284	285	287	288	289	291	292	296	299	335
A1	W	G	S	T	I	D	E	H	E	V	L	N	R	Y	N	N	R	L	E	F	L	Y	Y	N	K	K	D	T	K	K
A2	W	G	S	T	I	D	E	H	D	V	L	N	R	Y	N	N	R	L	E	F	L	Y	Y	N	K	K	D	T	K	K
A3	W	G	S	T	I	D	E	H	D	V	F	N	R	Y	N	N	R	L	K	F	R	D	Y	D	Q	N	I	N	E	K
A4	W	G	G	K	I	D	E	D	D	V	L	N	R	Y	N	N	R	L	E	F	L	Y	Y	N	K	K	D	T	K	R
A5	W	G	S	T	I	D	E	H	D	V	L	N	R	Y	N	N	R	L	E	F	L	Y	Y	N	K	K	D	T	K	K
A6	W	G	S	T	I	D	E	H	E	V	L	N	R	Y	N	N	R	L	E	F	L	Y	Y	N	K	K	D	T	K	K
A7	W	G	S	T	I	D	E	H	D	V	L	N	R	Y	N	N	R	L	E	F	L	Y	Y	N	K	K	E	I	K	K
A8	W	G	S	T	I	D	E	H	D	V	L	N	R	Y	N	N	R	L	E	F	L	Y	Y	N	K	K	D	T	K	K
consensus>70	W	G	s	t	I	D	E	h	#	V	l	N	R	Y	N	N	R	L	e	F	l	y	Y	#	k	k	d	t	k	k

L JLI-G10

	% ID	% SIM
B1		
B2	88.46	88.46
B3	88.46	88.46
B4	69.23	80.77
B5	96.15	96.15
B6	88.46	88.46
B7	73.08	84.62
B8	76.92	84.62

	1021	1104	1105	1189	1190	1240	1242	1244	1247	1248	1249	1250	1251	1263	1266	1269	1270	1271	1272	1273	1275	1276	1277
B1	K	G	N	E	E	I	H	R	Y	G	I	V	F	E	Y	W	Y	E	R	K	P	Y	N	K	L	G
B2	K	G	N	E	E	I	H	R	Y	G	I	V	L	K	Y	W	Y	E	R	K	P	Y	N	N	L	G
B3	K	G	N	K	E	I	H	R	Y	G	I	V	F	K	Y	W	Y	E	R	K	P	Y	N	N	L	G
B4	T	G	N	Q	E	I	H	R	Y	G	V	L	R	K	Y	W	Y	E	R	K	P	Y	K	N	L	G
B5	K	G	N	E	E	I	H	R	Y	G	I	V	F	K	Y	W	Y	E	R	K	P	Y	N	K	L	G
B6	K	G	N	K	E	I	H	R	Y	G	I	V	F	K	Y	W	Y	E	R	K	P	Y	N	N	L	G
B7	K	G	N	Q	E	I	H	N	Y	G	I	L	F	K	Y	W	Y	E	K	K	P	Y	S	N	L	G
B8	K	G	S	K	E	I	H	R	Y	G	F	V	F	Q	Y	W	Y	E	K	K	P	Y	N	D	L	G
consensus>70	k	G	n	.	E	I	H	r	Y	G	i	v	f	k	Y	W	Y	E	r	K	P	Y	n	n	L	G

Figure S6. Sequence conservation of the VHH-binding epitopes across BoNT/A and BoNT/B subtypes. Related to Figures 2–4.

(A–F) LCH_N/A (A–C) or H_CB (D–F) is drawn in surface. Identical, conserved, and variable residues at the BoNT/A–VHH or BoNT/B–VHH interface are colored yellow, purple, and blue, respectively.

(G–L) Amino acid sequence alignment among BoNT/A (G–I) or BoNT/B (J–L) subtypes. Only the VHH-binding epitopes are shown. The percentage of sequence identity (%ID) and similarity (%SIM) are shown. Sequence alignments were performed using Clustal Omega and displayed with ESPript 3.0.

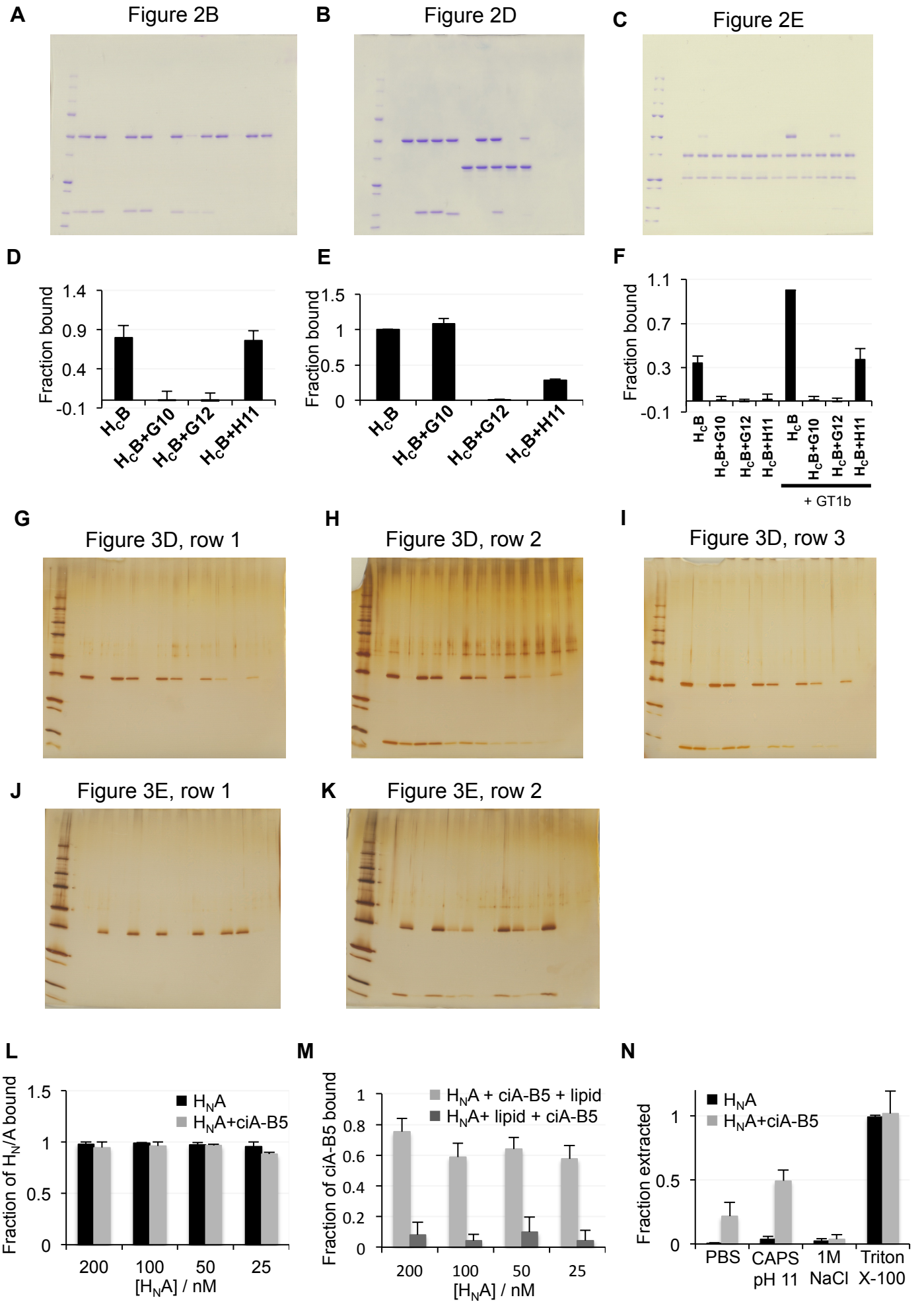
A
Figure 2B
B
Figure 2D
C
Figure 2E
D
Fraction bound
1.4
0.9
0.4
-0.1
HcB
HcB+G10
HcB+G12
HcB+H11
E
Fraction bound
1.5
1
0.5
0
HcB
HcB+G10
HcB+G12
HcB+H11
F
Fraction bound
1.1
0.7
0.3
-0.1
HcB
HcB+G10
HcB+G12
HcB+H11
HcB
HcB+G10
HcB+G12
HcB+H11
+ GT1b
G
Figure 3D, row 1
H
Figure 3D, row 2
I
Figure 3D, row 3
J
Figure 3E, row 1
K
Figure 3E, row 2
L
Fraction of HN/A bound
1.5
1
0.5
0
HNA
HNA+ciA-B5
200
100
50
25
[HNA] / nM
M
Fraction of ciA-B5 bound
1
0.8
0.6
0.4
0.2
0
HNA + ciA-B5 + lipid
HNA+ lipid + ciA-B5
200
100
50
25
[HNA] / nM
N
Fraction extracted
1
0.5
0
HNA
HNA+ciA-B5
PBS
CAPS pH 11
1M NaCl
Triton X-100

Figure S7. Uncropped images and quantification of data shown in Figures 2–3.
(A–C) Uncropped images for data shown in Figure 2.
(D–F) Quantification of results shown in Figure 2B, 2D, and 2E.
(D) The intensities of protein bands were quantified for the input and the supernatant fractions. The fraction of the bound-H_CB was calculated as 1 − (band intensity of unbound protein / input protein).
(E) The band intensities of the bound H_CB in the presence of VHH were quantified and represented as (Intensity / Intensity of binding of H_CB alone).
(F) The band intensities of the bound H_CB were quantified and represented as (Intensity / Intensity of binding of H_CB with GST-Syt II in the presence of GT1b).
(G–K) Uncropped images for data shown in Figure 3.
(L–N) Quantification of results shown in Figure 3D–E.
(L) The band intensities of H_NA were quantified for the input and the supernatant fractions.
(M) The band intensities of ciA-B5 were quantified. The fraction of the bound-protein was calculated as 1 − (band intensity of unbound protein / input protein).
(N) The band intensities of H_NA were quantified for the pellet fraction without treatment and the resuspended soluble fraction (S2). The fraction of the extracted protein was calculated as a ratio of band intensities of H_NA after and before extraction. The data are presented as mean ± S.D., n = 3.

Protein[A]	Subunit[B]	Neutralization[C]	EC_{50} (nM) [D]
JEQ-H11	Hc	No	0.2
JFM-A11[E]	Hc	Yes	0.6
JFM-B9	Hc	No	0.8
JFN-B5	Hc	No	0.4
JLI-G10[E]	Hc	Yes	0.3
JLI-H11	Hc	Yes	10*
JLJ-F9	Lc	No	10*
JLJ-G3	Lc	No	0.7
JLK-D7	Hc	No	0.1
JLK-G12	Hc	Yes	0.5
JLO-C8	Hc	No	1*
JLO-G7	Lc	No	1*
JLO-G11	Hc	Yes	0.5
JLU-D10	unknown	Yes	2*
JLU-H9	unknown	No	trace*
JLU-H10	unknown	No	0.1
JNE-B10	Lc	No	1

Table S1. A summary of anti-BoNT/B VHH characterization data. Related to Figures 1–2.

[A] Lab code given to each VHH.

[B] Subunit recognition was assessed by ELISA with purified BoNT light chain (LC) or heavy chain C-terminus (H_C). VHHs recognizing BoNT holotoxin without recognition of purified LC or H_C are indicated as unknown (likely H_N or LCH_N).

[C] VHH neutralization was determined by the ability of VHHs (20 nM) to clearly inhibit VAMP cleavage following overnight incubation of primary neurons with 1 nM BoNT/B1.

[D] The EC_{50} was the VHH concentration that produced about 50% of the peak signal on a serial dilution ELISA on ciBoNT/B1-coated Costar plates.

[E] JFM-A11 reported in our earlier study is clonally related to JLI-G10 while JLI-G10 displayed a higher binding affinity to BoNT/B1 than JFM-A11 (Mukherjee et al., 2012), therefore we focused on JLI-G10 in this study.

* These VHHs improved to sub-nM EC_{50} in ELISAs when BoNT/B1 was captured onto plastic plates with an antibody, suggestive of conformation-dependent epitopes.

Table S2. Data collection and refinement statistics. Related to Figures 1–4.

	H_CB–JLI-G10	H_CB–JLK-G12	H_CB–JLI-H11	H_CB–JLO-G11	LCH_N/A–B5–D12–H7	LCH_N/A–D12/11/B5–H7
Data collection						
Space group	P 63	C 1 2 1	P 1	C 2 2 21	C 1 2 1	C 1 2 1
Cell dimensions						
a, *b*, *c* (Å)	223.1, 223.1, 58.49	153.24, 53.19, 114.41	71.21, 73.28, 76.37	56.30, 267.90, 144.69	141.04, 89.36, 143.69	141.3, 90.25, 144.8
α, *β*, *γ* (°)	90, 90, 120	90, 92.35, 90	87.83, 65.75, 66.55	90.00, 90.00, 90.00	90, 118.93, 90	90, 119, 90
Resolution (Å)	111.57–2.20 (2.24–2.20)[a]	38.28–2.90 (3.08–2.90)	44.58–2.32 (2.39–2.32)	144.69–3.18 (3.40–3.18)	37.74–2.20 (2.25–2.20)	47.21–2.02 (2.05–2.02)
R_{merge}	0.096 (0.722)	0.120 (0.611)	0.055 (0.484)	0.153 (1.843)	0.049 (0.208)	0.094 (0.716)
CC1/2	0.994 (0.733)	0.964 (0.684)	0.997 (0.810)	0.990 (0.376)	0.997 (0.965)	0.995 (0.648)
I/σ(I)	10.2 (2.0)	7.4 (1.7)	13.9 (2.2)	8.5 (0.8)	10.2 (3.7)	9.8 (2.0)
Completeness (%)	99.2 (99.9)	96.7 (97.9)	98.6 (97.8)	99.0 (98.3)	95.0 (97.5)	99.8 (99.9)
Redundancy	4.9 (5.0)	3.2 (3.3)	3.9 (3.8)	3.6 (3.6)	2.6 (2.6)	3.7 (3.8)
Refinement						
Resolution (Å)	96.63–2.20	38.28–2.90	37.48–2.32	45.38–3.18	37.16–2.20	47.21–2.02
No. reflections	84236	20026	54471	18355	75238	103988
Reflections used for R_{free}	4213	1029	2764	865	3774	5185
R_{work}/R_{free}	0.194/0.211	0.212/0.258	0.170/0.222	0.204/0.258	0.181/0.229	0.183/0.195
No. atoms	9563	4621	9263	4599	10088	10407
Protein	9155	4597	8938	4599	9564	9608
Ligand/ion	-	10	-	-	-	-
Water	408	14	325	-	524	799
B-factors	46.2	47.3	52.00	99.60	34.90	37.50
Protein	46.3	47.2	52.20	99.60	34.70	37.20
Ligand/ion	-	97.7	-	-	-	-
Water	43.8	36.2	44.90	-	38.10	40.10
R.m.s. deviations						
Bond lengths (Å)	0.008	0.004	0.008	0.004	0.008	0.016
Bond angles (°)	1.120	0.697	1.018	0.810	1.09	1.446

One crystal was used for each structure.

[a] Statistics for the highest-resolution shell are shown in parentheses.

Table S3. A summary of the in vivo toxin neutralization studies of the designer VNAs. Related to Figures 5–7.

VNA	Distance / Å	Spacer length (a.a.)	Simultaneous binder?	BoNT LD_{50}	Survival at 96 hours (Alive / Tested)
ciA-D12…ciA-B5	17	11	Yes	100	10 / 10
				500	0 / 5
				1,000	0 / 5
				2,500	0 / 5
				10,000	0 / 5
ciA-D12…ciA-H7	92	11	No	100	1 / 10
				500	0 / 5
				1,000	0 / 5
				2,500	0 / 5
JLI-G10…JLI-G12	37	12	Yes	100	5 / 5
				200	5 / 5
				1,000	10 / 10
				5,000	2 / 5
				10,000	0 / 5
JLK-G12…JLI-G10	80	5	No	100	1 / 5
				200	0 / 5
				1,000	1 / 10
				5,000	1 / 5
JLI-H11…JLK-G12	61	20	Yes	100	5 / 5
				200	5 / 5
				1,000	10 / 10
				5,000	1 / 5
				10,000	2 / 5
		3	No	100	5 / 5
				200	5 / 5
				1,000	1 / 10
				5,000	2 / 5
				10,000	0 / 5